An SDR-Based Performance Measurement of LTE and WLAN Coexistence

Nadia Yoza-Mitsuishi, Yao Ma, and Jason Coder

National Institute of Standards and Technology, 325 Broadway, Boulder, Colorado, USA

***Abstract*— In this paper, we report on a software-defined radio (SDR) based test setup to emulate and evaluate the performance of two wireless coexistence scenarios. The first case we study consists of two long-term evolution (LTE) downlink channels from adjacent cells, and the second case is formed by an LTE downlink channel coexisting with a wireless local network (WLAN) channel. Different from available SDR measurement works, this test design provides new methods such as real-time adjustment of communication and inter-cell interference (ICI) channel gains, the measurement of SDR receiver internal noise power and noise figure, and the measurement of link signal-to-interference-and-noise ratio (SINR). We compare the measured LTE SINR-to-throughput mapping result with a theoretical upper bound which assumes 3GPP reference channel quality indicator (CQI) values and an ideal communication hardware. Our measurement results illustrate the SINR gap caused by the effects of imperfect SDR hardware and noise figure, and show interesting findings about LTE and WLAN performance under varying mutual interference conditions. Our SDR design and measurement methods can be extended to support the performance evaluation and optimization of more general multicell LTE and WLAN coexistence systems.**

***Index Terms*—Intercell interference, LTE, Noise figure, Spectrum sharing, Wireless coexistence, WLAN.**

I. Introduction

To support fast prototyping and system performance evaluation and optimization, software-defined radio (SDR)-based techniques have found widespread applications in emulating 4G long-term evolution (LTE), 5G and other systems [1]–[12].

The authors of [1] discussed capabilities and limitations of several open-source SDR tools for 5G system prototyping and evaluation. The works in [2]–[4] reported SDR-based performance evaluation of LTE license assisted access (LAA) schemes. Especially, [3] provided numerical comparisons between SDR measurement and Monte Carlo simulation results for LTE-LAA based system coexistence, and a close match was observed. A few signal sensing and spectrum monitoring schemes via SDR were reported in [5], [6]. The authors of [7] discussed the design and performance evaluation of an SDR phased array receiver which detected live LTE cellular signal and self-generated LTE signal, respectively. Measurement performance of signal power received by a smart phone was reported in [7]. To support the 5G system performance evaluation, the authors of [9] discussed the development and performance evaluation result of a 3D hybrid beamforming prototype. Furthermore, a few SDR based performance evaluation results of 5G non-orthogonal multiple access (NOMA) schemes were provided in [10], [11]. In [12], the LTE throughput via SDR was evaluated comprehensively for different channel bandwidths. The authors compared the LTE throughput-to-modulation coding scheme (MCS) mapping (reported by an open-source package [13]) with a theoretical upper bound based on 3GPP reference values [14]. However, the SINR-to-MCS mapping was not included and, therefore, a complete understanding of the SINR-to-throughput mapping was not provided.

Despite these works, the emulation of a multicell LTE network and its performance evaluation via an SDR technique has not been adequately studied or reported. Furthermore, the coexistence performance evaluation of LTE with wireless local network (WLAN) calls for additional research effort, to which SDR emulation could be applied. Emulation of LTE cells via low cost SDR devices generates practical value for deployment. Yet, available SDR configurations were not flexible enough to adjust the communication and interference channel quality in real-time to emulate the effect of diverse transmitter and receiver location profiles. Further, there is a lack of reporting on the LTE link SINR-to-throughput mapping via SDR measurement taking into account realistic hardware imperfections and noise figure.

In this paper, we implement an SDR and test circuit measurement, and provide a mapping between the SINR and the achieved key performance indicators (KPIs), such as link payload throughput and packet drop rate. The novel contributions of this work are highlighted as follows:

- We configure a two-cell LTE-based prototype via SDR and programmable multi-channel attenuators, which provide real time precise control of communication and inter-cell interference (ICI) channel gains. This supports the emulation of different eNB and UE locations (or distance profiles) and a fading channel environment.
- We measure the SDR and WLAN transmit and receive power levels and circuit losses, and the SDR internal noise. Using this result, we design a method to calculate the noise figure caused by the SDR internal noise, which is shown to be significant.
- We measure the LTE downlink SNR (and SINR)-to-throughput mapping, and compare it with a theoretical

*Certain commercial equipment, instruments, or materials are identified in this paper in order to adequately specify the simulation procedure. Such identification is not intended to imply recommendation or endorsement by the National Institute of Standards and Technology, nor is it intended to imply that the materials or equipment identified are necessarily the best available for the purpose.

upper bound (related with 3GPP reference values [14]) and another mapping reported by open-source SDR software [13]. The comparison illustrates the performance gap caused by hardware imperfections and other factors.
- Besides the coexistence test of two LTE links, we also measure the coexistence performance of an LTE link and a WLAN link, and provide some interesting findings.

Though we configure only a two-link model, the technique and results reported here can be extended to scenarios of multiple links or cells. Thus, this work can bring significant practical value to emulating and measuring the performance of 4G and 5G coexistence systems.

II. Test Setup of a Two-Cell Model

Let us consider a two-link licensed LTE model, where two eNodeB's (eNBs) transmit signals to each of the two user equipments (UEs), respectively, and have ICIs between the two downlink channels. We evaluate the licensed LTE performance in the measurement, but the setup and result can be extended to unlicensed LTE and 5G unlicensed new radio scenarios. The model configuration is shown in Fig. 1.

The purpose of this test is to check the impact of varying power levels of downlink channels and ICIs on the coexistence performance of two adjacent LTE cells. The measured performance metrics include downlink throughput and packet loss rate. The uplink throughput was also captured but is not shown in this paper due to the space limitation.

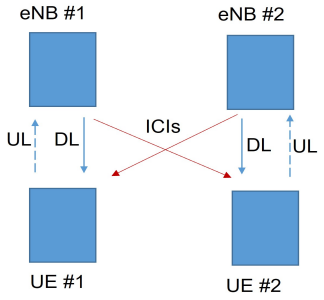

Fig. 1: Conceptual illustration of a two-cell LTE model, where the two downlink channels have mutual ICIs.

A detailed schematic configuration is shown in Fig. 2. For the coexistence measurement of two LTE downlinks, the two transmitters are eNBs, the two receivers are UEs, and each of them is emulated by an SDR universal software radio peripheral (USRP) device. For the LTE-WLAN coexistence test, the second link is replaced by a WLAN link using commercial-off-the-shelf (COTS) WLAN development boards, where the transmitter and receiver emulate an access point (AP) and a station (STA), respectively. A programmable 4-channel attenuator (e.g., Att_1,. . ., Att_4) controls the path gains of two communication links and two mutual interference links in real time. The test setup also includes two computers, four units of power combiner or splitter, fixed-value attenuators (shown by Att_0), RF cables, and other test circuitry. An additional SDR receiver (with an additional splitter) is used to capture the I/Q samples of the received RF signal to support both data processing and future spectrum sensing research. The configuration in Fig. 2 can be regarded as an extension of a two-link test scheme proposed in [3].

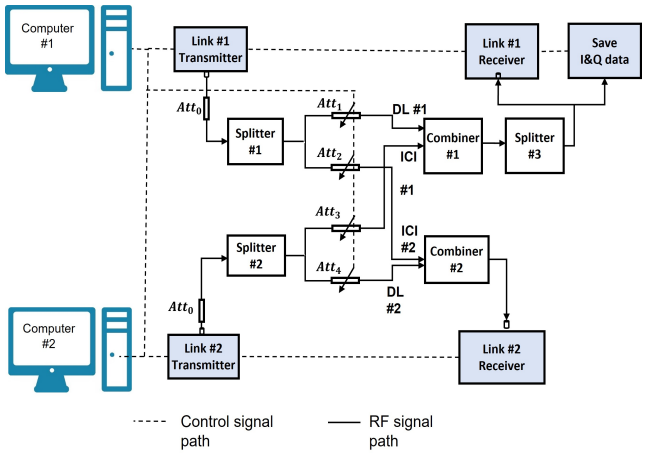

Fig. 2: SDR test configuration which emulates a two-cell ICI model.

The LTE emulation software consists of a popular open-source SDR package [13] which provides eNB and UE functions, in addition to an evolved packet core (EPC) running on the computers. The WLAN link is based on IEEE 802.11a/g with one spatial stream. The Wi-Fi AP and Wi-Fi client functions are implemented on development boards running an open-source software [15] for improved flexibility, which achieve a limited maximum payload throughput of 28 Mbps [16]. Our test software includes customized test-automation scripts such as:

- a function which measures KPIs including the payload throughput and packet loss rate,
- a function which changes the 4-channel programmable attenuator values online (as to change the communication and interference path gains),
- and a function which saves the KPI and ADC I/Q data in various formats.

We run throughput tests via an iperf software tool [17] on both LTE and WLAN links to capture the KPIs. A photo of part of our LTE downlink test setup is given in Fig. 3. It shows five SDR units (one is reserved for capturing I/Q samples), fixed-value attenuators, a programmable 4-channel attenuator, power splitters and combiners, and RF cables.

In our tests, the LTE and WLAN links are configured with channel bandwidths of 10 MHz and 20 MHz, respectively. For the case of two LTE links, both operate in a frequency-division duplexing (FDD) mode with a downlink center frequency of 2.68 GHz and an uplink center frequency of 2.56 GHz. For the case of one LTE and one WLAN link, both links operate at a central frequency of 5.22 GHz (which corresponds to Wi-Fi channel #44).

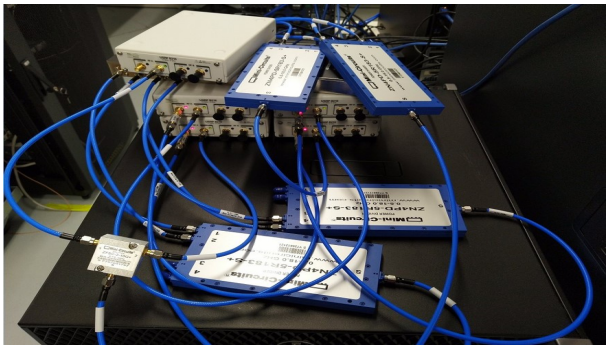

Fig. 3: Photo of part of our SDR test configuration.

III. SDR Internal Noise Measurement and Result

We implement both the test circuit and SDR measurements using a CW signal. Then we use the measurement result to estimate the noise figure caused by the SDR internal noise.

A. SDR Internal Noise Power

The intrinsic thermal noise power P_{AWGN} in an SDR receiver can be expressed as

$$P_{\text{AWGN}}(\text{dBm}) = -174 \text{ dBm/Hz} + N_F + 10\log_{10} B_w \text{ (Hz)}, \quad (1)$$

where N_F and B_w are the noise figure and noise effective bandwidth, respectively.

To estimate the N_F caused by the SDR internal noise, we consider a single LTE link without ICI. We turn off the transmitter and run a software program at the SDR receiver, which captures the I/Q samples and saves them to a host computer. We define $P_{I/Q,\min}$ as the average power of the digital I/Q signal when the input to the receiver is zero. In a linear scale, $P_{I/Q,\min} = P_{I/Q,sam} F_s$, where $P_{I/Q,sam}$ is the I/Q signal power per sample, and F_s is the ADC sampling rate, set to be equal to the bandwidth $B_w = 20$ MHz. $P_{I/Q,\min}$ provides a power estimate of the internal noise, and can be used to estimate the noise figure.

B. Test Circuit and SDR Measurement

First, we implement the test circuit measurement. The CW signal goes through the test circuitry from an SDR transmitter to a receiver, which includes a fixed attenuator with nominal value of 30 dB, a power splitter, a programmable attenuator, a combiner, and RF cables. We set the programmable attenuator value to change from 0 dB to 35 dB with 1 dB step size, and use a power meter to measure the transmit and receive power levels, and power losses in the circuitry. The transmit power $P_{\text{CW,TX}}$ (dBm) and received signal power $P_{\text{CW,RX}}$ (dBm) are related by

$$P_{\text{CW,RX}}(\text{dBm}) = P_{\text{CW,TX}}(\text{dBm}) - L_{\text{Cir}}(\text{dB}), \quad (2)$$

where L_{Cir} is the circuit loss, with $L_{\text{Cir}}(\text{dB}) = L_{\text{Cir,min}}(\text{dB}) + A_{\text{pro}}(\text{dB})$. Here, $L_{\text{Cir,min}}$ is the minimum circuit loss when the nominal value of the programmable attenuator is set to zero, and A_{pro} is the nominal value of the programmable attenuator which is adjustable from 0 to 95 dB.

Second, we implement an SDR internal circuitry measurement. At the SDR receiver, the input RF signal goes through an internal circuit including a low noise amplifier (LNA), a mixer with local oscillator (LO), a digital down-converter (DDC), and an ADC, and is converted to I/Q samples.

The impact of this SDR internal circuitry to the signal quality, in terms of the noise figure, has to be adequately evaluated. Furthermore, the ADC I/Q samples alone do not provide adequate information about the input RF signal power. In order to relate the I/Q samples to the input signal power, we define a power conversion factor (F_{conv}) between the input RF signal power at receiver (P_{RX}) and the ADC I/Q-sample signal power $P_{I/Q}$, given by

$$F_{\text{conv}}(\text{dB}) = P_{\text{CW},I/Q}(\text{dB}) - P_{\text{CW,RX}}(\text{dBW}), \quad (3)$$

where $P_{\text{CW},I/Q} = P_{I/Q} - P_{I/Q,\min}$ is the CW I/Q-signal power, with the contribution caused by the SDR internal noise ($P_{I/Q,\min}$) being removed.

We change the programmable attenuation value A_{pro} from 0 to 50 dB with a step size of 10 dB, measure the $P_{\text{CW,RX}}$ (dBW) and $P_{\text{CW},I/Q}$ (dB), and evaluate the conversion factor F_{conv} (dB). Note that $P_{\text{CW},I/Q} = P_{\text{CW},I/Q,\text{sam}} F_s$ in a linear scale, where $P_{\text{CW},I/Q,\text{sam}}$ is the I/Q signal power per sample. The result is given in Table I, which shows that the F_{conv} is pretty stable for different input signal power levels. Also, note that the unit dBW in $P_{\text{CW,RX}}$ relates to power in the RF domain while dB in $P_{\text{CW},I/Q}$ refers to the power in digital domain. Furthermore, when there is no confusion, we use a common unit dBm to denote the RF domain signal power and digital I/Q signal power, with $P(\text{dBm}) = P(\text{dBW}) + 30$ and $P(\text{dBm}) = P(\text{dB}) + 30$ respectively. The values of $P_{\text{CW},I/Q}$ appears high, which was caused by the factor F_s used therein.

We estimate the N_F of the SDR receiver based on average power spectral density outside of the signal bandwidth as

$$N_F(\text{dB}) = \text{PSD}_{\text{RX,min}}(\text{dBm}/Hz) - 174(\text{dBm}/Hz), \quad (4)$$

where $\text{PSD}_{\text{RX,min}}$ is the power spectral density (PSD) of the noise floor part of the input RF signal, and -174 dBm/Hz is the PSD of an ideal AWGN with $N_F = 0$ dB. Based on the

A_{pro} (dB)	$P_{CW,RX}$ (dBW)	$P_{CW,I/Q}$ (dB)	F_{conv} (dB)
0	-73.89	56.31	130.20
10	-83.89	46.50	130.39
20	-93.89	36.59	130.47
30	-103.88	26.69	130.57
40	-113.81	17.20	131.01
50	-123.11	7.50	130.61

TABLE I: List of SDR RF-to-I/Q conversion factor F_{conv} (dB) for different input signal powers, when $F_s = 20$ Msps.

CW measurement, we obtain that

$$\text{PSD}_{\text{RX,min}}(\text{dBm}) = \text{PSD}_{I/Q,\text{min}}(\text{dBm}) - F_{\text{conv}}(\text{dB}). \quad (5)$$

To compute the PSD of a digital signal, we utilize a time-domain average-and-smooth FFT process. In detail, we divide the time domain signal in many equal-sized segments. For each segment, we compute its periodogram via an FFT-and-square operation. Then we average over all the periodograms to obtain a smoothed PSD result. Our SDR noise figure measurement procedure is summarized below:

1) Capture I/Q samples at an SDR receiver when the transmitter is turned off, and evaluate the internal noise I/Q-sample power $P_{I/Q,\text{min}}$.
2) Turn on the transmitter, and measure and calculate the received RF powers at the SDR receiver. Record the I/Q samples and evaluate both RF power and I/Q power in pairs.
3) Evaluate the conversion factor using (3) as a function of different received powers.
4) Evaluate the noise figure using (4) as a function of different received powers.

We provide the PSDs (dBm/Hz) of the internal noise and noisy CW signal in Fig. 4, which shows a substantial gap between the intrinsic receiver noise floor and the ambient thermal noise (AWGN) floor. This corresponds to $N_F \simeq 12.9$ dB. According to [18], the SDR receiver N_F is about 17 dB when the operating center RF is set to be 2.68 GHz and the receiver gain is set to be 39 dB. Note the N_F in (4) is evaluated using a conducted test when the receiver input is zero, and it does not model the amplification of the external noise caused by the SDR receiver circuit. Thus, it gives a lower bound of the actual noise figure, such as that reported in [18].

In Fig. 5, we show the PSDs of I/Q samples of internal noise, the noisy LTE signal, and the PSD of a simulated pure LTE signal, when A_{pro}= 10 dB (without using the conversion factor). The simulated LTE signal was generated using a software (Matlab LTE toolbox) with 10 MHz bandwidth under

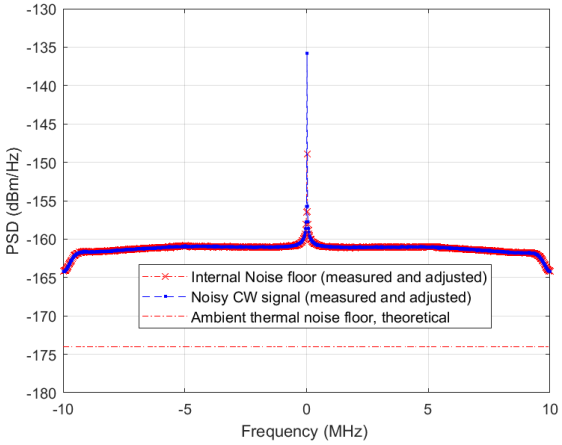

Fig. 4: PSDs of the internal noise and the noisy CW signal after the conversion factor adjustment, when A_{pro}= 50 dB.

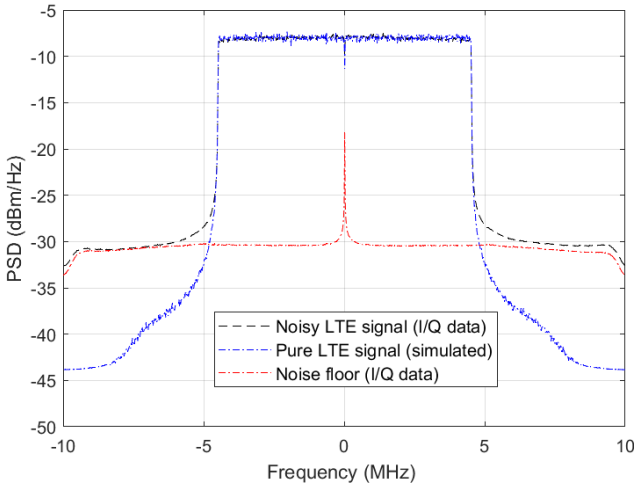

Fig. 5: PSDs of the I/Q samples of the internal noise (red line) and the noisy LTE signal (black line), and the PSD of a simulated pure LTE signal, when A_{pro}= 10 dB.

15.36 Msps sampling rate, and then resampled at $F_s = 20$ Msps. It is also rescaled in power so that its total power is equal to that of noisy LTE signal being studied. Based on 50 resource blocks in 10 MHz bandwidth, the LTE signal has a 9 MHz effective signal bandwidth. Yet, in the (-10 to -4.5) MHz and (4.5 to 10) MHz frequency ranges, the noisy LTE signal has a PSD that is significantly higher than that of the pure LTE signal, which could be caused by the SDR internal noise and hardware imperfection. By applying the result in Table I, and using a comparison with the AWGN noise floor (similar to that implemented for Fig. 4), we obtain an estimate that $N_F \simeq 13.1$ dB.

In our measurement, let P_0 be the signal power evaluated by integrating the signal PSD over the $B_{w,\text{LTE}} = 9$ MHz bandwidth, i.e., within the $(-4.5, 4.5)$ MHz range. The noise power is estimated by $N_0 = \overline{\text{PSD}}_{N_0} B_{w,\text{LTE}}$, where $\overline{\text{PSD}}_{N_0}$ is the average PSD at the edge region from $(-10, -7)$ and $(7, 10)$ MHz ranges. Since $P_0 = S_0 + N_0$, we estimate the SNR using the PSD result by $\text{SNR} = \frac{P_0}{N_0} - 1$.

IV. Coexistence Test Results

A. SINR Estimation

The SINR to LTE throughput mapping table used in the open-source LTE package is provided in the second column of Table II.

1) Both LTE links transmit signals using iperf tests. Measure the KPIs (such as throughput) of link #1 under interference of link #2.
2) Change the ICI channel attenuation value in both links from 32 dB to 0 dB in 1 dB stepsize (10 seconds of measurement at each step). The communication attenuation A_{pro} remains in 0 dB. Save throughput and packet loss result for each dB step.
3) Calculate link #1's SINR of each operating point and pair the SINR and KPI values by using the time stamp.

4) By repeating steps 1 to 3 above, measure link 2's SINR-to-KPI mapping.

B. SINR (or SNR) to the Payload Throughput Mapping

We obtain the SINR-to-LTE downlink throughput mapping of the SDR units by running iperf tests while changing the mutual downlink interference gains in the programmable attenuator.

Based on Section 7.1 of [14], we can obtain the mapping from the channel quality indicator (CQI) and number of physical resource blocks N_{PRB} to the transport block size (TBS) indexes $(0, 1, \ldots, 26)$ and the TBS payload throughput. The 10 MHz bandwidth we used for LTE links correspond to $N_{\text{PRB}} = 50$. Further, a CQI is mapped to a spectral efficiency (SE) value for the physical layer throughput (which does not count for the losses caused by physical and MAC layer overheads). However, the SINR to throughput mapping was not specified.

Based on [19], to achieve a given SE under 10% of block error rate, the required minimum SINR is approximately given by

$$\gamma_{\text{SINR}} = (2^{K_s \text{SE}} - 1)/\mathcal{L}, \tag{6}$$

where typical values of modeling parameters are $K_s = 1.25$ and $\mathcal{L} = 0.66$ [19]. Note that (6) does not model hardware imperfections.

SINR (best case) (dB)	SINR (soft-ware) (dB)	CQI	SE (bps/ Hz)	MCS	Payload throughput (kbps)
-6.7	1.95	1	0.15	0	1384
-4.7	4	2	0.23	1	1800
-2.3	6	3	0.38	3	2856
0.2	8	4	0.6	5	4392
2.4	10	5	0.88	7	6200
4.3	11.95	6	1.18	9	7992
5.9	14.05	7	1.48	12	9912
8.1	16	8	1.91	14	12960
10.3	17.9	9	2.41	16	15264
11.7	20.9	10	2.73	19	18336
14.1	22.5	11	3.32	22	22920
16.3	24.75	12	3.9	24	27376
18.7	25.5	13	4.52	27	31704
21	27.3	14	5.12	28	36696
22.7	29	15	5.55	28	36696

TABLE II: List of the mapping relations between the SINR of the best case (performance upper-bound), the SINR used in the open-source LTE software, the CQI, the SE, the MCS and the payload throughput, when an LTE link has a channel bandwidth of 10 MHz without interference.

In Table II we provide mappings among SINR, CQI, SE, MCS and payload throughput. The columns 1, 3, and 4 were the same as that given in [19]. The first column was calculated assuming an ideal SINR-and-throughput mapping given by Eq. (6). The 3rd column relates to the CQI defined in the 3GPP standard [14]. The SE in the 4th column corresponds to the physical layer raw throughput, and the last column provides the achieved payload throughput.

In Fig. 6, the SDR measured SNR-to-throughput mapping is compared with the best-case mapping, and the mapping reported by the open-source LTE package [13], which utilized an SNR-to-CQI mapping table given in [20]. The result in Fig. 6 shows that the measured mapping matches reasonably well with the software-reported mapping, except some operating points at a low SNR. For example, the SNR gap was around 4-5 dB when the throughput was at about 1 Mbps.

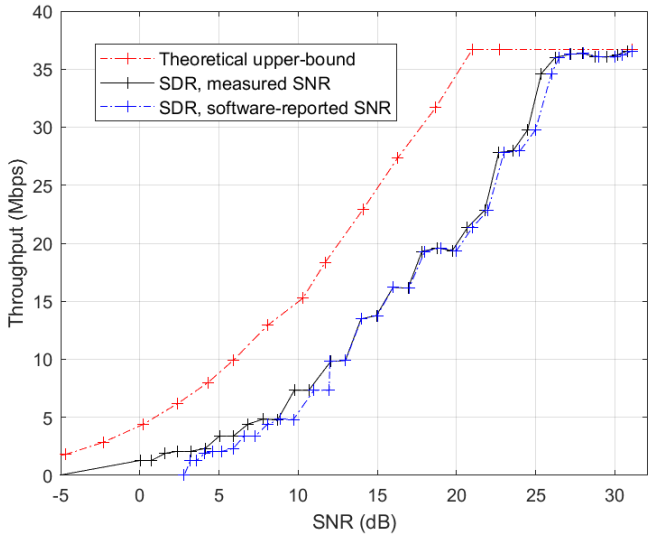

Fig. 6: Throughput vs. SNR in an LTE downlink scenario.

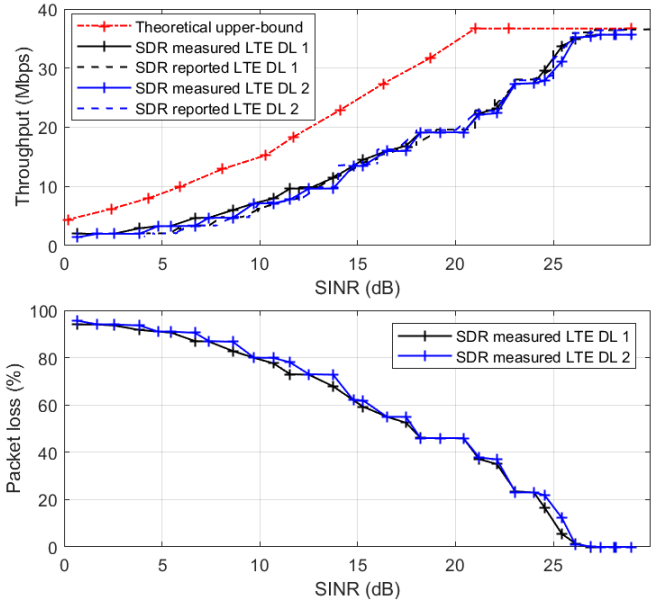

Fig. 7: Throughput and packet loss rate vs. SINR in a two-cell LTE downlink scenario.

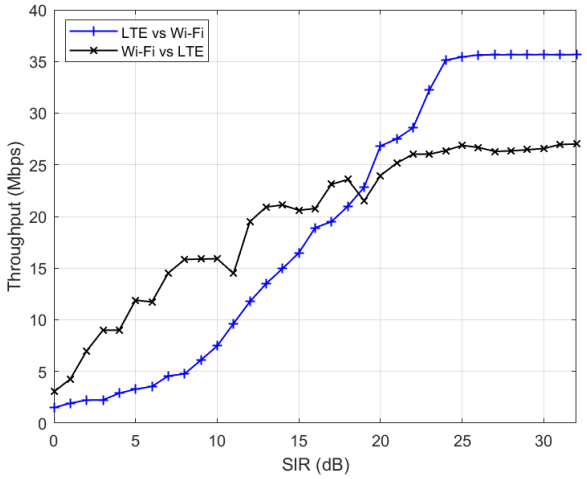

Fig. 8: Measured throughput vs. SINR in a coexisting LTE downlink and Wi-Fi downlink scenario.

C. Coexisting LTE links

In Fig. 7 we show the SDR measured throughput (solid curves) vs. SINR of the two LTE downlinks. We compare them with the theoretical upper-bound given in Table II (semi-dashed curve) and the throughput reported by the open-source LTE package (dashed curves). The measured and reported SINR-to-throughput mapping values are similar. Yet in a low SINR region, to achieve the same throughput, the measured SINR is lower than the software-reported SINR by 1.5 to 4 dB. Our method measures the powers of the received signal (at the ADC output) and ICI to calculate an SINR, while the open-source LTE software uses an LTE reference signal that goes through a raised cosine (RC) filter after the ADC to estimate the SINR (and SNR). This causes some differences in the SINR (and SNR) evaluation results.

Fig. 7 also compares the packet loss rate measured with the SDR for both LTE downlinks. Both of them are very similar and follow the same trend as in the throughput plots, with less percentage of packet loss for higher SINR values.

D. Coexisting LTE and WLAN links

In Fig. 8 we show the SDR measured LTE throughput and the WLAN downlink throughput using COTS boards, when the signal-to-interference ratio (SIR) changes from 0 to 32 dB. We observe that as the SIR increases, the LTE throughput increases monotonically, while the WLAN throughput has significant fluctuations at the SIR values of 11 dB, 19 dB and other places. This is likely caused by the channel sensing and transmission backoff algorithm used in the WLAN link, which is sensitive to competing LTE transmissions.

V. Conclusion

In this paper, we have provided an efficient SDR configuration and measurement method for performance evaluation of an LTE two-cell system and an LTE-WLAN coexistence system. Measurement results suggest a significant noise figure caused by the SDR internal noise. Taking into account the SDR internal noise, we provide a measured SINR-to-KPI mapping, and show the SINR gap between SDR performance and the performance upper-bound (assuming ideal hardware). Results also demonstrate effects of mutual interferences and hardware imperfections to KPIs of the coexistence systems. In a future work, we will configure and emulate 5G coexistence system with multiple cells, and implement both conducted and radiated tests. Furthermore, the measurement uncertainty will be evaluated and reported.

Acknowledgment

The authors would like to thank Dr. Dan Kuester for the discussions on SDRs and digital signal processing.

References

[1] F. Gringoli, P. Patras, C. Donato, P. Serrano, and Y. Grunenberger, "Performance assessment of open software platforms for 5G prototyping," *IEEE Wirel. Commun.*, vol. 25, no. 5, pp. 10–15, 2018.

[2] NI, "Real-time LTE/Wi-Fi coexistence testbed," 2019. [Online]. Available: https://www.ni.com/en-us/innovations/white-papers/16/real-time-lte-wi-fi-coexistence-testbed.html

[3] Y. Ma, R. Jacobs, D. G. Kuester, J. Coder, and W. Young, "SDR-based experiments for LTE-LAA based coexistence systems with improved design," in *IEEE GLOBECOM*, 2017.

[4] S. Bräuer, A. Zubow, and F. Dressler, "Towards software-centric listen-before-talk on software-defined radios," in *IEEE WCNC*, 2021.

[5] J. Milheiro, L. Almeida, J. P. Borrego, N. Borges Carvalho, and H. Kokkinen, "LTE signal detector for LSA spectrum sharing model in Portugal," *IEEE Trans. Veh. Technol.*, vol. 69, no. 12, 2020.

[6] R. Helbet, P. Bechet, S. Miclaus, and A. Sarbu, "Real time broadband electromagnetic spectrum monitoring system based on software defined radio technology," in *Int. Conf. Mod. Power Syst.*, 2021.

[7] Y. Boussad, M. N. Mahfoudi, A. Legout, L. Lizzi, F. Ferrero, and W. Dabbous, "Evaluating smartphone accuracy for RSSI measurements," *IEEE Trans. Instrum. Meas.*, vol. 70, pp. 1–12, 2021.

[8] Y. Boussad, A. Legout, W. Dabbous, L. Lizzi, F. Ferrero, and M. N. Mahfoudi, "Open-source 4G experimental setup," in *IEEE Int. Symp. Antennas Propag. North Am. Radio Sci. Meet.*, 2020, pp. 1399–1400.

[9] J. Jang, M. Chung, S. C. Hwang, Y.-G. Lim, H.-j. Yoon, T. Oh, B.-W. Min, Y. Lee, K. S. Kim, C.-B. Chae, and D. K. Kim, "Smart small cell with hybrid beamforming for 5G: theoretical feasibility and prototype results," *IEEE Wirel. Commun.*, vol. 23, pp. 124–131, 2006.

[10] X. Xiong, W. Xiang, K. Zheng, H. Shen, and X. Wei, "An open source SDR-based NOMA system for 5G networks," *IEEE Wirel. Commun.*, vol. 22, no. 6, pp. 24–32, 2015.

[11] X. Wei, H. Liu, Z. Geng, K. Zheng, R. Xu, Y. Liu, and P. Chen, "Software defined radio implementation of a non-orthogonal multiple access system towards 5G," *IEEE Access*, vol. 4, pp. 9604–9613, 2016.

[12] B. Maqsood, "Implementation and performance analysis of software defined radio (SDR) based LTE platform for truck connectivity application," Ph.D. dissertation, KTH, 2019.

[13] SRS, "Software Radio Systems (SRS) project, release 21.04." [Online]. Available: https://www.srslte.com/srslte-srsran

[14] 3GPP TSG RAN, "Evolved Universal Terrestrial Radio Access (E-UTRA) Physical layer procedures (Release 17), 3GPP TS 36.213 V17.0.0," 2021.

[15] OpenWrt, "OpenWrt Project, release 15.05.1." [Online]. Available: https://openwrt.org/

[16] B. Mafakheri, L. Goratti, R. Abbas, S. Reisenfeld, and R. Riggio, "LTE/Wi-Fi coordination in unlicensed bands: an SD-RAN approach," in *IEEE Conf. Netw. Softwarization*, 2019.

[17] iperf. [Online]. Available: https://iperf.fr/

[18] Ettus, "B210 USRP." [Online]. Available: https://kb.ettus.com/B200/B210/B200mini/B205mini

[19] A. Ghosh and R. Ratasuk, *Essentials of LTE and LTE-A*. Cambridge University Press, 2011.

[20] M. Kawser, N. Imtiaz Bin Hamid, M. N. Hasan, M. S. Alam, and M. M. Rahman, "Downlink SNR to CQI mapping for different multiple antenna techniques in LTE," *Int. J. Inf. Electron. Eng.*, vol. 2, no. 5, pp. 756–760, 2012.